RSC Advances

PAPER

View Article Online
View Journal | View Issue

Cite this: *RSC Adv.*, 2026, **16**, 20257

A novel environmentally friendly approach for ultra-trace determination of erbium in alloys and environmental samples

Yasmeen G. Abou El-Reash,[a] Amnah Al Zbedy,[b] Alaa M. Younis[c] and Alaa S. Amin *[d]

Received 22nd March 2026
Accepted 11th April 2026

DOI: 10.1039/d6ra02354a

rsc.li/rsc-advances

A novel, environmentally benign optical sensor membrane has been developed for the ultra-trace determination of erbium (Er^{3+}) in alloys and environmental samples. The sensor incorporates norfloxacin (NFX) and cetylpyridinium chloride (CPC) into a chitosan–silica composite (2 : 1 volume ratio) prepared *via* an optimized sol–gel process. The resulting sensor demonstrated excellent selectivity at pH 9.3 and exhibited a response time of three minutes. A linear response was observed for concentrations spanning from 5×10^{-6} to 7.5×10^{-9} M, with a correlation coefficient (r^2) of 0.9975. The limit of detection (LOD) and limit of quantitation (LOQ) were determined to be 2.2×10^{-9} M and 7.3×10^{-9} M, respectively. Precision and accuracy assessments showed a relative standard deviation (% RSD) of 1.46 and a recovery percentage (% recovery) of 100.96%. Along with its high stability and reproducibility, the sensor exhibited remarkable selectivity for Er^{3+} ions over common cations. The optode was successfully applied to Er^{3+} analysis in alloys, binary mixtures, and water samples.

Introduction

Rare earth elements (REEs), comprising the fifteen lanthanides along with scandium and yttrium, were first identified as a distinct group of seventeen chemical elements by Carl Axel Arrhenius in 1787 and subsequently classified into two principal categories based on their atomic weights.[1] The most widespread REE-bearing minerals are monazite ((Ce, La, Nd, Th)$PO_4 \cdot SiO_4$), bastnaesite ((Ce, La)(CO_3)(OH, F)), and xenotime (YPO_4). Monazite and bastnaesite constitute the primary origins of light REEs and together supply approximately 95% of the rare earth elements currently in use, whereas xenotime is mainly associated with the heavier REEs.[2,3]

Given that many lanthanides are products of nuclear fission, the development of sensitive methods for detecting trace concentrations of these ions in environmental matrices such as seawater is of critical importance. Erbium, a member of the lanthanide series within group IIIb of the periodic table, exhibits an abundance of approximately 2.8 mg kg^{-1} in the Earth's crust and 0.9 mg L^{-1} in seawater,[4] ranking it approximately 45th in crustal elemental abundance.[5] Although erbium and its compounds demonstrate low acute toxicity, they present hazards through inhalation of dust or fumes and ingestion, potentially causing irritation to the eyes, skin, and respiratory tract. As a lanthanide, erbium can interfere with calcium metabolism, accumulate in bone and liver tissue, and at elevated concentrations, impair cellular respiration, enzyme activity, and induce oxidative stress. While erbium compounds are rarely encountered in everyday exposure, they should be regarded as highly toxic, with metal dust presenting fire and explosion hazards.

Erbium possesses diverse practical applications across multiple fields. It functions as a photographic filter and serves as a durable metallurgical additive. In nuclear technology, erbium is employed in neutron-absorbing control rods. Within optical communications, erbium-doped silica glass fibers constitute the active medium in erbium-doped fiber amplifiers (EDFAs) and fiber lasers, typically co-doped with glass modifiers such as phosphorus or aluminum to prevent clustering. High-power Er/Yb fiber lasers utilize fibers co-doped with both erbium and ytterbium, while erbium is also applied in erbium-doped waveguide amplifiers.[6]

In latest years, numerous techniques have been created to establish the concentration of individual rare earth elements in the samples of seawater from diverse sites. These include voltammetry,[7] potentiometric ion-selective electrodes,[8–10] Rutherford backscattering methods,[11] mass spectrometry,[12] preconcentration followed by ICP-MS, and neutron activation analysis (NAA).[13,14] Additionally, greater-order derivative spectrometric approaches for the detection of Er^{3+} ions have been documented.[14–17] Despite their analytical utility, many of these

[a]*Department of Chemistry, College of Science, Imam Mohammad Ibn Saud Islamic University (IMSIU), P.O. Box 90950, 11623 Riyadh, Saudi Arabia*
[b]*Chem. Depart., Al-Qunfudah Universiy College, Umm Al-Qura University, Al-Qunfudah 1109, Saudi Arabia*
[c]*Department of Chemistry, College of Science, Qassim University, Buraidah, 51452, Saudi Arabia*
[d]*Chemistry Department, Faculty of Science, Benha University, Benha, Egypt. E-mail: asamin2005@hotmail.com*

techniques are constrained by limitations including narrow operational concentration ranges, significant interferences from coexisting cations, and relatively high detection limits.

Optical chemical sensors represent a promising approach for heavy metal detection, typically incorporating colorimetric complexing agents within polymeric membranes.[18–24]

Over the past decade, analytical chemistry has seen rapid advancement in optical chemosensors for metal ion detection, favored for their selectivity, simple fabrication, enhanced sensitivity, and elimination of reference electrode requirements compared to electrochemical sensors.[25–27]

Chitosan–silica composite membranes offer a promising matrix for optical sensor development. The inherent fragility and limited biocompatibility of silica are ameliorated by chitosan incorporation,[28] while silica enhances the structural stability and pore integrity of chitosan-based membranes.[29] This feature is particularly significant for optode membranes, as the presence of pores facilitates metal adsorption.[30] Chitosan–silica membranes have found applications in biomedical, pharmaceutical, biosensing, and adsorption fields. Additionally, their combination of porosity and mechanical robustness makes them suitable for biosensors aimed at detecting compounds such as uric acid and dopamine.[31]

The sol–gel technique provides an effective method for optode membrane fabrication, enabling synthesis at moderate temperatures for both purely inorganic materials and inorganic–organic hybrids. This approach offers superior mechanical stability, minimal chemical reactivity, ambient temperature processing, and broad substrate compatibility.[32] To date, only limited reports exist of highly selective spectrophotometric optical sensor membranes for aqueous erbium determination.[9,33,34]

Norfloxacin (NFX) has been previously suggested as a reagent for the derivative spectrophotometric analysis of erbium.[35] The characteristic absorption band appeared at 523 nm, with Beer's law being valid from 5.0×10^{-5} M. In this work, we introduced a modification by developing a novel optode based on norfloxacin to enhance both selectivity and sensitivity through complex formation with Er^{3+} ions. Accordingly, we explored the incorporation of this reagent into chitosan membranes for subnanomolar detection of erbium ions in aqueous media.

Experimental

Apparatus

A Fisons (UK) dual glass distillation apparatus was employed to produce deionized water. The pH readings were conducted using a Jenway 3505 pH meter, which operated on a 9 V AC power supply. The spectroscopic measurements were performed with the JASCO 530V UV-vis spectrophotometer. The absorption tests were undertaken by positioning the membrane inside a quartz cuvette, and in batch mode, the values were taken, with the temperature maintained at a controlled 25 ± 2.0 °C. The readings from both the air and a blank optode sample were contrasted with the absorbance measurements of the optode samples. In addition to, the PerkinElmer model 5300 DV instrument, located in Waltham, MA, USA, was employed to perform all ICP-AES (Inductively Coupled Plasma-Atomic Emission Spectroscopy) measurements.

Reagents and solutions

Analytical-grade reagents were used throughout all experiments, with deionized water serving as the solvent in all cases. Ethanol was used to dissolve 0.2925 g of NFX (purity 99.85%, dried to constant weight at 105 °C), and the resulting solution was then diluted with ethanol to a final volume of 100 mL to prepare a 7.5×10^{-3} M stock solution of NFX. Appropriate quantities of Er^{3+} oxide (99.99% pure, Aldrich) were dissolved in small volumes of concentrated nitric acid to prepare stock solutions, which were then diluted with distilled water. Standardization was performed following procedures reported in the literature.[36] Working standard solutions of erbium were subsequently obtained by appropriate dilution in the required medium.

Lanthanide solutions (0.01 M) were made by dissolving the suitable quantity of the oxide (spectrographically standardized, Johnson Matthey, Royston, Hertfordshire, UK) in a 1 : 1 mixture of hydrochloric acid, and working solutions were subsequently obtained by diluting with water.

A 7.5×10^{-3} M cetylpyridinium chloride (CPC; Fluka AG, Buchs SG) solution was prepared by dissolving 0.6713 g in 250 mL distilled water. An ammonia–ammonium chloride buffer (pH 9.35) was formulated by mixing 117 mL of 0.5 M ammonia with 83 mL of 0.5 M ammonium chloride; working buffer solutions were prepared by serial dilution with distilled water.

Safety precautions

All experiments involving Er^{3+} ions were conducted with appropriate glove protection due to their high toxicity. Waste solutions containing Er^{3+} were carefully collected and disposed of to prevent environmental contamination.

Procedure

Synthesis of chitosan–silica membrane and immobilization of NFX and CPC. The chitosan–silica membrane was prepared through a multi-step process. A silica sol was first prepared by mixing tetraethyl orthosilicate (TEOS; 22.2 mL), ethanol (22.2 mL), deionized water (88.8 mL), and 0.1 M HCl (5.0 mL), followed by stirring for 24 h with a magnetic stirrer. Separately, a 3.0% (w/v) chitosan solution was obtained by dissolving 3.0 g chitosan in 100 mL of 2.0% acetic acid and stirring for 3 h. The silica sol was then combined with the chitosan solution at chitosan-to-silica volume ratios of 1 : 3, 1 : 2, 1 : 1, 2 : 1, or 3 : 1, with continued stirring for 2 h. The homogeneous mixture was cast onto a glass plate and dried at ambient temperature to form the chitosan–silica membrane. For demolding, the membrane was immersed in 1.0% NaOH solution and rinsed with deionized water to neutrality.[29]

The membrane was subsequently immersed in an ethanolic solution of NFX and CPC (7.5×10^{-3} M each) for 6 h to achieve immobilization, followed by rinsing with deionized water for 12 h.[37]

Assessment of chitosan–silica membrane characteristics. Membrane characteristics were evaluated using Fourier transform infrared (FTIR) spectroscopy to identify functional groups and scanning electron microscopy (SEM) to examine surface morphology of both pristine chitosan and chitosan–silica membranes. Prior to SEM observation, the membrane surface was coated with a thin layer of gold for 40 minutes, allowing detailed visualization.

Assessment of performance and validation of the optode. The performance of the optode was examined by assessing its maximum absorption wavelength, optimal pH, and response time to Er^{3+} ions. Measurements were undertaken employing a UV-vis spectrophotometer. A 1 × 1 cm optode was immersed in an Er^{3+} solution until its color transitioned from colorless to red. Afterward, the optode was removed, dried, and placed in a cuvette holder. Its absorbance was then recorded over the visible wavelength interval of 350–650 nm to identify the peak value.[38]

The optode was exposed to a solution containing Er^{3+} ions under different pH conditions and time intervals to determine the optimal pH and response duration. The pH range investigated spanned from 2.5 to 11, while the exposure time varied between 1.0 and 6.0 min.

The optode validation involved assessing its linear response, detection and quantification limits, selectivity, precision, accuracy, and sensitivity.[38–40] For the selectivity evaluation, transition and lanthanide metal ions were employed as potential interfering species.

Sample procedure

Permanent magnet. A 0.1 g synthetic sample was dissolved in HCl to achieve 6.0 M final acid concentration and diluted to 1.0 L with deionized water. An aliquot containing Er^{3+} was analyzed following the general optode procedure.

Superconductor material. A 0.1 g synthetic sample was dissolved in concentrated HCl and diluted to 500 mL with deionized water, then digested on a steam bath for 6 h, cooled, and filtered. The precipitate was rinsed with hot water, and the filtrate was transferred to a 100 mL volumetric flask and diluted to volume with deionized water. An aliquot containing Er^{3+} was subjected to optode-absorptiometric analysis.

Results and discussion

Chitosan–silica membrane

For efficient extraction of Er^{3+} ions from aqueous media, the sol–gel membrane must exhibit mechanical strength, uniform composition, flexibility, and wear resistance while maintaining a sufficiently thin structure to enable rapid regeneration and effective removal of Er^{3+} ions post-analysis without compromising stability. These essential characteristics guided the optimization of membrane composition. To enhance selectivity, sensitivity, and membrane stability, the proportions of individual components were systematically optimized.

Chitosan–silica membranes were synthesized *via* sol–gel technique using chitosan-to-silica volume ratios of 1 : 1, 1 : 2, 1 : 3, 2 : 1, and 3 : 1. Membrane formation failed at ratios of 1 : 2 and 1 : 3, yielding fractured films. In contrast, continuous membranes were successfully obtained at ratios of 1 : 1, 2 : 1, and 3 : 1. Membrane formation was strongly influenced by the relative amounts of chitosan and silica; increasing the silica content hindered membrane integrity due to the inherent brittleness of silica. Conversely, excessive chitosan incorporation led to increased membrane opacity, which adversely affected optode measurements. An optimal chitosan–silica composition produced an optode membrane with adequate porosity, wear resistance and mechanical strength. Based on these observations, a chitosan-to-silica ratio of 2 : 1 was selected for membrane fabrication, as it yielded a sufficiently transparent, mechanically stable membrane without noticeable shrinkage.

Characteristics of chitosan–silica membrane

According to Al-Sagher and Salim,[41] interactions between silica and chitosan involve multiple bonding mechanisms (Scheme 1). Hydrogen bonding occurs between chitosan amide groups and silica silanol groups. Ionic interactions form between chitosan amino groups and silanol groups, while covalent linkages may develop through esterification reactions between chitosan hydroxyl groups and silica silanol groups.

FTIR analysis of the membrane revealed an absorption band at 3387 cm^{-1} attributed to overlapping N–H and O–H stretching vibrations.[42] The band at 2922 cm^{-1} corresponded to C–H stretching, 1586 cm^{-1} to C–N stretching, 1155 cm^{-1} to C–O–C stretching, and 1077 cm^{-1} to C–O stretching. These characteristic bands align with the reported FTIR spectrum of chitosan.[43]

The FTIR spectra of chitosan–silica and NFX-immobilized chitosan–silica membranes closely resembled that of pristine chitosan, exhibiting only minor wavenumber shifts and additional absorption bands. In the chitosan–silica membrane, the broad 3387 cm^{-1} band shifted to 3360 cm^{-1}, indicating intermolecular hydrogen bonding between silica hydroxyl groups and chitosan amino (N–H) groups.[29] Absorption bands detected at 1077 cm^{-1} were attributed to Si–O–Si stretching vibrations, while the band near 900 cm^{-1} corresponded to Si–OH groups.[42] Upon immobilization with NFX, new characteristic peaks emerged; the band at 3225 cm^{-1} was assigned to O–H stretching vibrations, whereas the absorption at 1725 cm^{-1} was related to the C=O stretching of carboxyl functional groups.[44]

SEM observations revealed that the pure chitosan membrane exhibited a compact and smooth morphology, with no discernible pores. Incorporation of silica into the chitosan matrix, as well as subsequent loading of NFX into the chitosan–silica composite, resulted in a rougher surface; however, the distribution of these components was non-uniform. The degree of silica dispersion across the chitosan surface was influenced by the stirring duration. Moreover, the silica particles displayed irregular morphologies due to the use of TEOS as the precursor, leading to surface particles with diverse shapes, including spherical, oval, rectangular, and triangular forms.[45] Upon NFX incorporation, the apparent particle size increased, as the silica particles on the chitosan surface became coated with NFX. The drug was able to diffuse onto the chitosan–silica membrane,

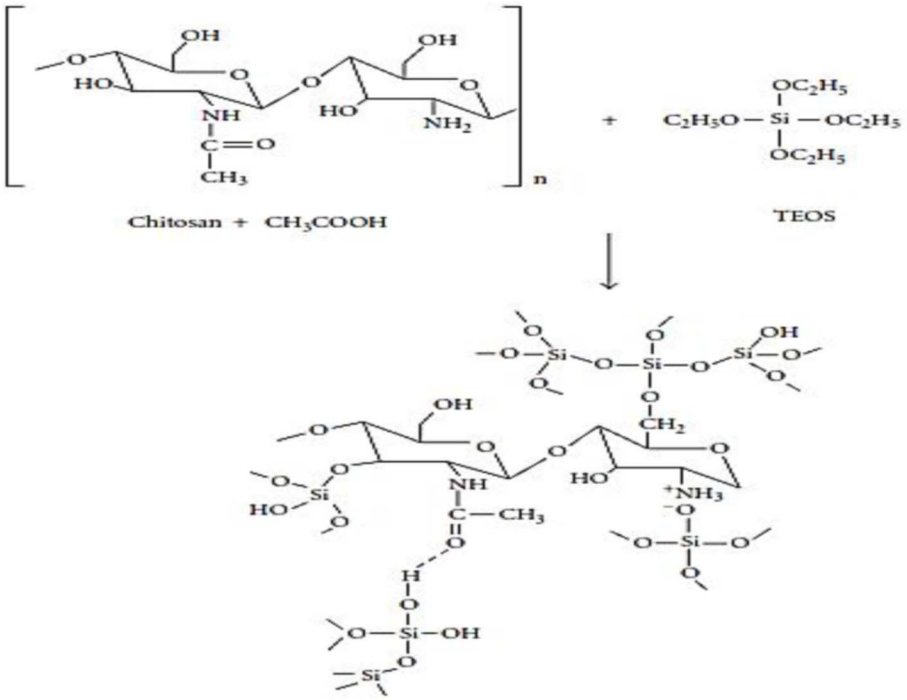

Scheme 1 Schematic structure model of chitosan–silica membrane.

and because the membrane was fabricated *via* the sol–gel technique, NFX could be effectively adsorbed onto the composite surface.[46]

Immobilization of NFX and CPC on chitosan–silica membrane

NFX and CPC were immobilized by immersing the chitosan–silica membrane in 7.5×10^{-3} M ethanolic NFX/CPC solution. The resulting membrane appeared colorless (Scheme 2). The diffusive properties of NFX and CPC enabled penetration and adsorption within membrane pores, rendering them effective Er^{3+} sensing agents.

Optode of Er^{3+}

The performance of the immobilized membrane was evaluated using different concentrations of Er^{3+} solution. NFX and CPC formed a colored Er^{3+}-NFX complex, inducing a visible colorless-to-red transition. Complexation occurs *via* coordination of Er^{3+} with NFX hydroxyl and carboxyl oxygen atoms (Scheme 2).[35] The recorded maximum absorbance values at varying Er^{3+} concentrations are illustrated in Fig. 1. The optode membrane exhibited its highest absorbance at a wavelength of 544 nm. This value differs from the previously reported maximum wavelength of 523 nm,[35] which can be attributed to variations in the membrane composition used for optode fabrication, leading to a shift of the maximum wavelength.

Complex formation and stability were pH-dependent, with maximum NFX–Er^{3+} stability at pH 9.3 (Fig. 2). In the acidic–

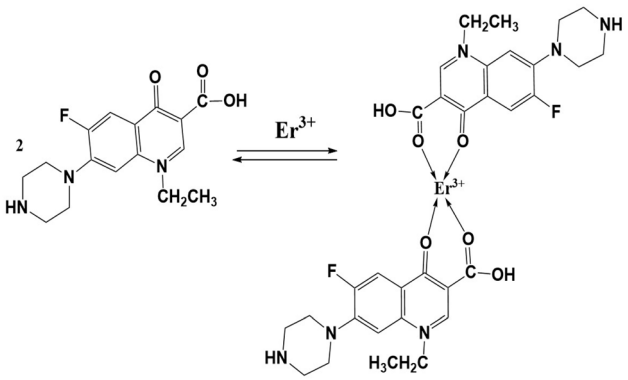

Scheme 2 Reaction of complex formation of NFX with Er^{3+}.

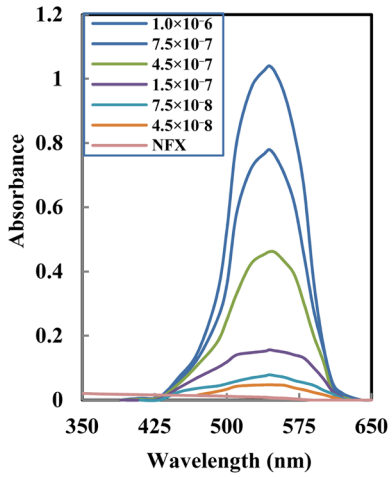

Fig. 1 Absorption spectra of NFX and its Er^{3+} complexes with various [Er^{3+}] at pH 9.3.

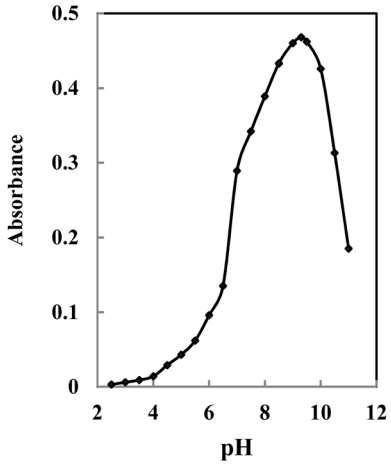

Fig. 2 Effect of pH on the response of the proposed optode; conditions: $[Er^{3+}] = 4.5 \times 10^{-7}$ M.

neutral range (pH 3–7), protonation of oxygen donor atoms weakened donor–acceptor interactions, destabilizing the complex. Stable complexation occurred at pH 8.0–9.5. Beyond this range, absorbance decreased due to Er^{3+} hydroxide formation and precipitation (Fig. 2). The interaction period among the optode membrane and the Er^{3+} solution was maintained within a range of 3.0–6.0 min (Fig. 3). Maximum response was achieved at 3.0 min, when Er^{3+} fully interacted with immobilized NFX. This response is markedly faster than triacetyl cellulose-based optodes requiring 20–25 min for stabilization.

Effect of surfactant

The experimental findings demonstrated that both cationic surfactants (cetylpyridinium chloride (CPC) and cetyltrimethyl ammonium bromide (CTMAB)) and non-ionic surfactants (Triton X-100 and Tween-80) enhanced 4f electron transitions of the complexes. Anionic surfactant DBSS caused precipitation and was unsuitable. CPC was selected due to superior solubility relative to CTMAB (Fig. 4).

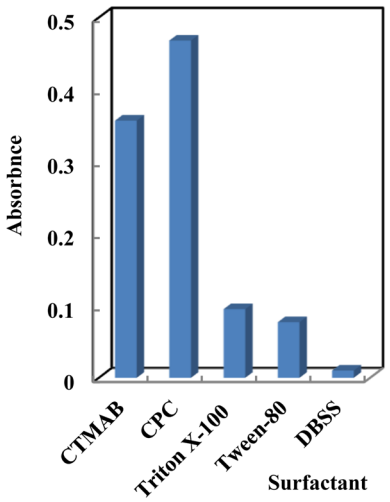

Fig. 4 Effect of surfactant on the response of the proposed optode; conditions: $[Er^{3+}] = 4.5 \times 10^{-7}$ M.

Sensor stability and response time

In the optode designed with the ideal composition, the response time is influenced by the duration required for the analyte to move from the primary solution to the interface of the optode membrane, where it interacts with the NFX. The calculation of response time was conducted by monitoring the variation in absorbance as the solution shifted from ammonia buffer at pH 9.3 to a buffered solution with 4.5×10^{-7} M Er^{3+} ions. It was observed that the optode membrane reached 97.5% of its total absorbance in approximately 2.0 minutes for the maximum concentrated solution, and around 3.0 minutes for the most diluted one. The sensor remained stable in aqueous solutions with a pH lower than 9.3 for a minimum of 12 hours. During the first 12 hours of immersion in an ammonia buffer solution with a pH of 9.3, the membrane's absorbance was measured every hour, yielding a standard deviation of 1.46% for $n = 12$ readings. This suggests no leakage of NFX throughout this period. No change in absorbance was observed when the

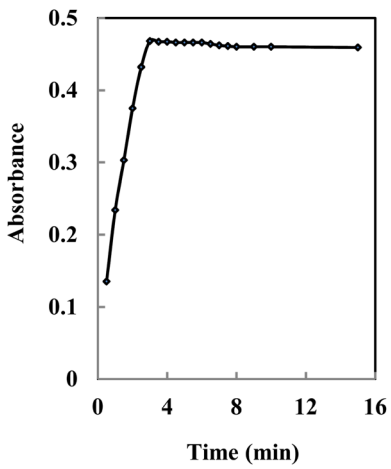

Fig. 3 Effect of contact time of optode membrane using 4.5×10^{-7} M.

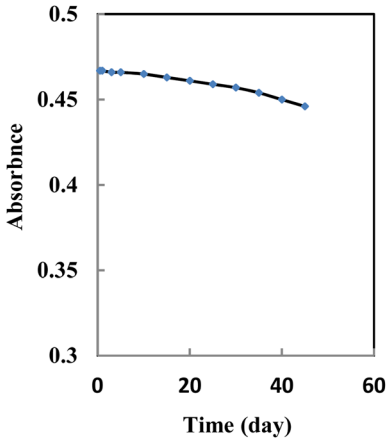

Fig. 5 Stability of the proposed optode used for $[Er^{3+}] = 4.5 \times 10^{-7}$ M at the optimum conditions.

Table 1 Tolerance ratio (TR = ion/Er^{3+} mass ratio) for various interfering ions in the determination of 4.5×10^{-7} M of Er^{3+}

Ion	TR	RE (%)	Ion	TR	RE (%)
Na^+, Li^+, NH_4^+	20 000	−3.5	Fe^{2+}, Fe^{3+}, oxalate	7000	−3.2
K^+, Tl^+, Ag^+, NH_3	18 000	−3.3	Pd^{2+}, Hg^{2+}, SO_4^{2-}	6000	4.0
Ca^{2+}, Mg^{2+}, citrate	16 500	−3.7	Sn^{2+}, Cd^{2+}, SCN^-	5000	−3.6
Sr^{2+}, Ba^{2+}, succinate	15 000	−3.5	Co^{2+}, Te^{4+}, Se^{4+}, Cl^-	4000	−4.5
Ge^{4+}, Ti^{4+}, PO_4^{3-}	13 500	−4.3	Sn^{4+}, Zn^{2+}, acetate	3000	3.3
Bi^{2+}, Mn^{2+}, NO_2^-	12 000	4.3	Cu^{2+}, Ni^{2+}, CO_3^{2-}	2250	3.1
Mo^{6+}, W^{6+}, IO_3^-	15 000	−3.0	Au^{3+}, Cr^{3+}, HCO^{3-}	1500	3.9
Cr^{6+}, UO_2^{2+}, $B_4O_7^{2-}$	9000	−3.6	Al^{3+}, Eu^{3+}, Lu^{3+}	1000	4.4
Gd^{3+}, Zr^{4+}, Pt^{4+}, Br^-	8000	3.7	Sc^{3+}, La^{3+}, Tb^{3+}, Ho^{3+}, Nd^{3+}	350	4.6

optode membrane was subjected to light, and the membrane maintained its stability during the experiment with no signs of NFX seepage. Additionally, the membrane optode showed no alterations over a 45-days period as shown in Fig. 5, when left idle and maintained in surrounding air.

Reproducibility and repeatability

Optode reproducibility and repeatability represent key performance metrics. Repeatability was assessed by multiple immersions in 4.5×10^{-7} M Er^{3+}, yielding absorbance % RSD = 1.46% at 544 nm ($n = 10$). Reproducibility across six membranes with 4.5×10^{-7} M Er^{3+} yielded % RSD = 1.75% at 544 nm. These results confirm excellent reproducibility and repeatability.

Selectivity of optode

A major characteristic of the given optode membrane is its selectivity, which demonstrates its ability to preferentially signify the primary ion rather than other ions coexisting in the solution. The selectivity of the proposed optical sensor toward Er^{3+} ions was systematically evaluated by introducing a variety of potentially interfering metal ions into a solution containing 4.5×10^{-7} M of Er^{3+} under optimized conditions. An interference was defined as a deviation of ±5.0% in the recovery relative to a Er^{3+} solution without additional ions. Therefore, the optode selectivity was assessed by introducing interfering metal ions into the test solution. The metal ions employed in this work were alkali, transition, heavy, and lanthanide.

A study was carried out to evaluate how various common alkali, transition, heavy, and lanthanide ions affect the absorbance of the developed Er^{3+} optode. To determine the selectivity of the Er^{3+} sensor, the absorbance of a constant level of Er^{3+} ions (4.5×10^{-7} M) in a solution with a pH of 9.3 was measured both before (A_0) and following (A) the introduction of potentially interfering ions, at concentrations up to 350 times of the analyte ion. The relative error (RE%) is calculated using the formula:

$$\mathrm{RE}(\%) = [(A - A_0)/A_0] \times 100.$$

Despite chemical similarities among rare earths, interferent effects on Er^{3+} absorbance remained minimal under optimized conditions, with all RE values < 4.6% (acceptable range). Negligible positive interference occurred with Ho^{3+} and Nd^{3+}. Additional examination indicated that ions such as NH_4^+, CH_3COO^-, NO_3^-, $C_2O_4^{2-}$, CO_3^{2-}, NO_2^-, BO_3^-, IO_3^-, and borax, even at increased concentrations up to 1500 times, did not demonstrate significant interference with the Er^{3+} assay (Table 1). The results indicate that the optode demonstrated strong selectivity for Er^{3+} ions, enabling it to accurately detect low levels of Er^{3+} in both natural environmental, industrial sludge and alloy samples, even when various other cations and anions are present. Furthermore, the optode provides the benefits of a rapid response time and is suitable for use across a broad range of concentrations.

Regeneration of the sensor

Optode absorbance did not fully revert upon transfer from high to low Er^{3+} concentrations. Regeneration efficiency was tested with EDTA, NaOH, H_2SO_4, HCl, and HNO_3. HNO_3 (≥0.01 M) proved most effective, completely removing bound Er^{3+} within 2.0 min and restoring baseline absorbance (Fig. 6). Post-regeneration, membranes required 3.0 min immersion in pH 9.3 ammonia buffer prior to reuse. The membrane can be regenerated up to four times without any degradation of its properties. After each regeneration, the optode must be sited in a buffer solution for 1.0 to 3.0 minutes before measuring the next Er^{3+} concentration.

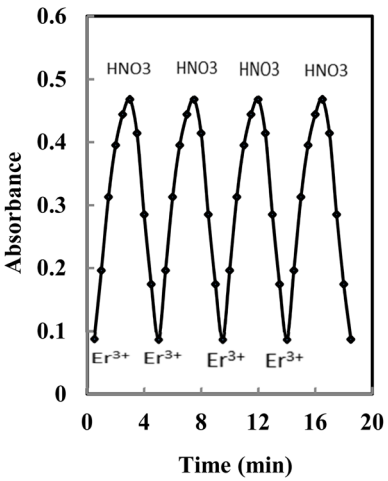

Fig. 6 Reversibility of the optode exposed 4.5×10^{-7} M Er^{3+} and 0.05 M HNO_3.

Table 2 Analytical features of the proposed method

Parameters	Sol–gel sensor
pH	9.3
Optimum [NFX] (M)	7.5×10^{-3} M
Chitosan: Silica ratio	2 : 1
Reaction time (min)	3.0
Beer's range (M)	5×10^{-6}–7.5×10^{-9}
Ringbom range (M)	4×10^{-6}–2.5×10^{-8}
Molar absorptivity (L mol^{-1} cm^{-1})	1.04×10^{6}
Sandell sensitivity (ng cm^{-2})	0.016
Intercept	
Slope	6.44
Intercept	−0.009
Correlation coefficient (r)	0.9975
RSD[a] (%)	1.46
Detection limits (M)	2.2×10^{-9}
Quantification limits (M)	7.3×10^{-9}

[a] Average of six determinations.

Analytical figure of merit

All elevated parameters ascribed previously are used so as to make Er^{3+} calibration curve. The calibration graph established on absorbance of the sol–gel thin film *versus* Er^{3+} ion concentration was linear in the range of 5×10^{-6}–7.5×10^{-9} M with equation of $A = -0.009C + 6.44$ and correlation coefficient (R^2) of 0.9975, where C is concentration of Er^{3+} in μg mL^{-1} and A is absorbance of sol–gel thin film at 544 nm. The RSD, and limits of detection and of quantification based on three and ten times the standard deviation of blank[47] were 2.2×10^{-9} and 7.3×10^{-9} M were listed in Table 2.

The reliability of the suggested procedure is essential for the development of the optode and also serves as one of the verification assessments. Accuracy is expressed as the percentage ratio among the determined concentration and the true concentration. In this study, acceptable accuracy values ranged from 97.33 to 103.33 for concentrations measured in μM. Subsequently, the analysis included computing the percentage recovery. The % recovery values for every concentration, as presented in Table 3, fell within the range considered to indicate good accuracy.

The performance of the recommended sensor membrane was evaluated against various earlier spectral techniques[47–51] (Table 4). The suggested sensor membrane is distinguished by its quick response time and its applicability across a wide range of concentrations. It exhibits a strong selectivity for Er^{3+} ions compared to lanthanide and transition metal ions, fulfilling the necessary selectivity coefficients for identifying Er^{3+} ions in alloys, binary mixtures, and water samples.

Analytical application

Due to the exceptional selectivity and subnanomolar detection limit of the developed Er^{3+} optode, it was applied to quantify Er^{3+} ions in various binary mixtures. The findings, presented in Table 5, denote that the recoveries of Er^{3+} ions across all mixtures ranged from 97.7% to 102.5%, demonstrating the acceptable performance and the extreme level of erbium selectivity achieved by the suggested optode. A t-test was performed[52]

Table 3 Calculation result of accuracy optode, replicate $n = 6$

	Measured [Er] (M)				
Replicates [Er] (M)	Proposed	ICP-AES	Recovery (%)	t-Test[a]	F-Value[a]
1.5×10^{-8}	1.55×10^{-8}	1.43×10^{-8}	103.33	1.79	
4.5×10^{-8}	4.40×10^{-8}	4.65×10^{-8}	97.68		3.53
7.5×10^{-8}	7.60×10^{-8}	7.40×10^{-8}	101.33	1.95	
1.5×10^{-7}	1.46×10^{-7}	1.55×10^{-7}	97.33		4.08
4.5×10^{-7}	4.60×10^{-7}	4.65×10^{-7}	102.33	2.07	
7.5×10^{-7}	7.40×10^{-7}	7.65×10^{-7}	98.67		4.22
1.5×10^{-6}	1.54×10^{-6}	1.42×10^{-6}	102.67	1.86	
5.0×10^{-6}	4.90×10^{-6}	5.13×10^{-6}	98.00		2.94

[a] Theoretical values for t and F at 95% confidence limit are 2.57 and 5.05, respectively.

Table 4 Comparison of the present method with other spectrophotometric methods

Reagent	pH	λ_{max} (nm)	ε ($\times 10^4$)	Beer's μg mL^{-1}	Ref.
5-(2′,4′-Dimethylphenylazo)-6-hydroxypyrimidine-2,4-dione	8.5–9.0	635	669.7	0.0005–0.125	30
1-(2-Pyridylazo)-2-naphthol	7.5–8.0	538	5.0	1.0–7.0	49
2-(3,5-Dichloro-2-pyridylazo)-5-dimethylaminophenol	6.8	375	13.9	1.0–4.5	50
2-(3,5-Dichloro-2-pyridylazo)-5-dimethylaminophenol	2.5	584	12.7	0.02–2.0	51
2-(Diphenylacetyl)indan-1,3-dione	10.0	446	1.13	0.1–25.1	52
2-(5-Bromo-2-pyridylazo)-5-diethylaminophenol	9.0–10.9	581	13.6	0.02–1.3	53
Norfloxacin	9.2–9.5	523	1.92	8.4–42.0	36
Norfloxacin	9.3	544	104.0	0.001–0.836	This work

Table 5 The Er^{3+} ions recovery from binary mixtures by the proposed Er^{3+}-optode

		Found[a] (ng mL^{-1})				
Er^{3+} (ng mL–1)	Added cation (ng mL^{-1})	Proposed	ICP-AES	Recovery (%)	*t*-Test[b]	*F*-Value[b]
50	Ce^{3+}, 250	49.3	52.0	98.6[a] ± 0.5	1.32	2.78
30	Ho^{3+}, 150	30.5	29.0	101.7 ± 0.6	1.59	3.46
60	Lu^{3+}, 300	61.0	58.2	101.7 ± 0.7	1.44	3.29
80	Tb^{3+}, 400	79.0	82.4	98.8 ± 0.3	1.65	3.82
100	Pr^{3+}, 500	102.5	97.2	102.5 ± 0.6	1.28	2.53
70	La^{3+}, 350	69.1	92.3	98.7 ± 0.4	1.48	3.50
40	Sc^{3+}, 200	41.0	38.7	102.5 ± 0.5	1.72	4.17
120	Mg^{2+}, 600	118.6	123.2	98.8 ± 0.6	1.40	3.07
150	Na^{+}, 750	153.7	146.8	102.5 ± 0.7	1.69	4.03
180	Ca^{2+}, 900	177.7	184.0	98.7 ± 0.5	1.33	2.89
80	Co^{2+}, 400	79.0	81.2	98.8 ± 0.3	1.57	3.42
90	Cu^{2+}, 450	91.6	88.0	101.8 ± 0.6	1.60	3.75
110	Zn^{2+}, 550	107.5	112.2	97.7 ± 0.5	1.78	4.36
50	Fe^{3+}, 250	51.2	48.6	102.4 ± 0.7	1.65	3.97

[a] Results are based on six measurements. [b] Theoretical values for *t* and *F* at 95% confidence limit are 2.57 and 505, respectively.

to evaluate the outcomes of both methods, revealing no notable distinctions at a 95% confidence level. These results reinforce the dependability and precision of the engineered optode for erbium analysis across different samples.

The optode was further employed to monitor trace Er^{3+} concentrations in environmental water samples (tap, well, industrial, and river water from Benha, Egypt). Aliquots of 10 mL from each sample were transferred to 25 mL volumetric flasks and diluted with deionized water, followed by spiking with Er^{3+} standards (50–150 ng mL^{-1}). Er^{3+} levels were determined using the established calibration procedure. The results (Table 6) indicate near-quantitative recovery across all matrices. A *t*-test performed to evaluate the outcomes of both methods,[52] revealed no notable distinctions among the samples at a 95% confidence level. These results reinforce the dependability and precision of the engineered optical sensor for Er^{3+} ion analysis across different samples.

To evaluate the effectiveness of the suggested approach, the proposed optode was applied to determine Er^{3+} ions some erbium alloys. 0.1 g of erbium alloys ($Mg_{95}Al_3Er_2$ and $ErDy_4Al_{10}$ powder (from Sigma-Aldrich) was weighed carefully and transferred into a 50 mL beaker and then 10 mL of H_2SO_4 (10%) was added. The solution was stirred and heated (60 °C). Then, the pH was adjusted to 9.3 with ammonia buffer and the solution was filtered. The resulted solution was transferred into a 250 mL volumetric flask and the solution was made up to volume by deionized water. Then, the erbium content of 10 mL of this solution was analyzed by applying the presented optode using calibration method. The results are compared with the ICP-AES and shown in Table 7. Results agreed satisfactorily with ICP-AES values (Table 7).

The high selectivity and low detection limit also enabled Er^{3+} monitoring in synthetic samples mimicking Er^{3+} concentrates, including permanent magnet and superconductor material

Table 6 Ultra-trace detection of erbium in some environmental water samples

	Er^{3+} (ng mL^{-1})						
Sample	Added	Found[a]	ICP-AES	Recovery (%)	s_r (%)	*t*-Test[b]	*F*-Value[b]
Tap water	0.00	—	—				
	50.0	51.0	48.8	102.0	0.73	1.16	2.48
	100	98.2	105.0	98.2	0.85	1.34	2.79
Well water	0.00	—	—				
	60.0	60.8	58.7	101.3	0.71	1.27	2.61
	120	118.0	123.6	98.3	0.57	1.45	3.02
Industrial water	0.00	—	—				
	75.0	74.1	76.3	98.8	0.42	1.33	2.75
	150	153.4	146.9	102.3	0.37	1.57	3.28
Sea water	0.00	—	—				
	65.0	66.5	63.8	102.3	0.51	1.25	2.58
	130	127.6	133.9	98.2	0.38	1.40	2.88
River Nile	0.00	—	—				
	55.0	56.2	44.0	102.2	0.46	1.36	2.83
	110	107.5	122.6	97.7	0.75	1.60	3.47

[a] Average of six replicate determinations. [b] Theoretical values for *t* and *F* at 95% confidence limit are 2.57 and 5.05, respectively.

Table 7 Preconcentration and determination of Er^{3+} in synthetic samples

Sample	Er^{3+} added (μg mL^{-1})	Er^{3+} found[a] (μg mL^{-1})		Ref.
		Proposed[b]	ICP-AES[b]	
Permanent magnet, $Er_2Fe_{14}B$	0.49	0.50 ± 0.3	0.48 ± 1.4	53
Superconductor, $ErRh_4B_4$	0.45	0.44 ± 0.4	1.43 ± 1.4	54
$Mg_{95}Al_3Er_2$	—	47.3 ± 1.4	46.2[a] ±07	
$ErDy_4Al_{10}$	—	65.7 ± 1.2	63.2 ± 05	

[a] Average of six replicate determinations. [b] Standard deviation ($n = 6$).

compositions (Table 7). Optode results showed acceptable agreement with ICP–AES reference values, demonstrating practical applicability.

Conclusions

The newly developed Er^{3+} optical sensor demonstrates exceptional selectivity and sensitivity for ultra-trace detection. It provides a cost-effective, accurate alternative that eliminates complex extraction or preconcentration requirements.

Comprehensive optimization of experimental parameters—including surfactant selection, membrane thickness, stirring duration, chitosan/silica/NFX ratios, and pH—yielded superior analytical performance, with detection and quantification limits of 2.2×10^{-9} M and 7.3×10^{-9} M, respectively, across a linear range of 5×10^{-6} to 7.5×10^{-9} M.

Compared to existing methods, the proposed optode offers broader linear range, higher accuracy, superior stability, and reduced analysis time. Its selectivity minimizes interferences from diverse cations and anions. Successful application to alloys, binary mixtures, and water samples, with results statistically indistinguishable from ICP-AES (95% confidence), confirms its suitability for routine Er^{3+} monitoring in real matrices.

Author contributions

Yasmeen Abou El-Reash: conceptualization, investigation, data curation, methodology, visualization, validation, writing – original draft, writing– review & editing. Amnah Al Zbedy and Alaa Younis: conceptualization, data curation, investigation, methodology, validation, writing – original draft, writing – review & editing. Alaa Amin: conceptualization, methodology, data curation, investigation, supervision, validation, writing – original draft, writing – review & editing.

Conflicts of interest

There is no conflicts of interest

Data availability

The authors declare that the data supporting the findings of this work are available within the article.

Acknowledgements

This work was supported and funded by the Deanship of Scientific Research at Imam Mohammad Ibn Saud Islamic University (IMSIU) (grant number IMSIU-DDRSP2601).

References

1 N. G. Connelly, T. Damhus, R. M. Hartshorn and A. T. Hutton, *Nomenclature of Inorganic Chemistry*, International Union of Pure and Applied Chemistry, Biddles Ltd, King's Lynn, Norfolk, UK, 2005.
2 P. W. Harben, and M. Kuzvart, *Industrial Minerals: A Global Geology*, Industrial Minerals Information Ltd, 1996, p. 462.
3 T. Christie, B. Brathwaite and A. Tulloch, *Mineral Commodities Report 17 – Rare Earths and Related Elements*, Institute of Geological and Nuclear Sciences Ltd, New Zealand, 1998.
4 P. Patnaik, *Handbook of Inorganic Chemical Compounds*, McGraw-Hill, 2003, pp. 293–295, ISBN 0-07-049439-8.
5 F. H. Spedding and S. Jaffe, Conductances, solubilities and ionization constants of some rare earth sulfates in aqueous solutions at 25 °C, *J. Am. Chem. Soc.*, 1954, **76**, 882–884, DOI: 10.1021/ja01632a073.
6 J. Emsley, *Nature's Building Blocks: an A-Z Guide to the Elements*, Oxford University Press, US, 2001, pp. 181–182, ISBN 0-19-850341-5.
7 M. S. Zakharov and E. V. Vorobeva, Voltametric behavior of erbium and lutecium ions in solutions of alkali-halides, *Zh. Anal. Khim.*, 1994, **49**, 875–878.
8 M. R. Ganjali, M. Rezapour, S. Rasoolipour, P. Norouzi and M. Adib, Application of pyridine-2-carbaldehyde-2-(4-methyl-1,3-benzothiazol-2-yl) hydrazone as a neutral ionophore in the construction of a novel Er(III) sensor, *J. Braz. Chem. Soc.*, 2007, **18**, 352–358, DOI: 10.1590/S0103-50532007000200016.
9 M. R. Ganjali, F. Faridbod, P. Norouzi and M. Adib, A novel Er(III) sensor based on a new hydrazone for the monitoring of Er(III) ions, *Sens. Actuators, B*, 2006, **120**, 119–124, DOI: 10.1016/j.snb.2006.01.050.
10 F. Faridbod, M. R. Ganjali, P. Norouzi, B. Larijani, S. Riahi and F. S. Mirnaghi, Lanthanide recognition: an asymetric erbium microsensor based on a hydrazine derivative, *Sensors*, 2007, **7**, 3119–3135, DOI: 10.3390/s7123119.

11 V. Perina, J. Vaick, V. Hnatowicz, J. Cerena, P. Kolarova, J. Spirkova-Heradilova and J. Schrofel, RBS measurement of depth profiles of erbium incorporated into lithium niobate for optical amplifier applications, *Nucl. Instrum. Methods Phys. Res., Sect. B*, 1998, **139**, 208–212.

12 H. Holzbrecher, U. Brever, M. Gastel, J. S. Becker, H. J. Dietze, I. Beckers, S. Bauer, M. Elenster, W. Zander, J. Schubeat and C. Buehar, Fresenius, quantitative simsanalysis of erbium profiles in $LiNbO_3$, *J. Anal. Chem.*, 1995, **383**, 785–788, DOI: 10.1007/BF00321371.

13 V. M. Biju and T. P. Rao, Spectrofluorometric determination of erbium in seawater with 5,7-diiodoquinoline-8-ol and rhodamine 6G, *Anal. Sci.*, 2001, **17**, 1343–1345, DOI: 10.2116/analsci.17.1343.

14 K. R. Bandi, A. Upadhyay, A. K. Singh and A. K. Jain, Nano-level monitoring of Er(III) by fabrication of coated graphite electrode based on newly synthesized Schiff base as neutral carrier, *Mater. Sci. Eng., C*, 2016, **62**, 9–17, DOI: 10.1016/j.msec.2016.01.035.

15 N. X. Wang, Z. K. Si, J. H. Yang, W. Jiang, W. A. Liang, Z. D. Li, G. Y. Du and G. Zhang, Selective determination of neodymium and erbium in mixtures with other lanthanides by second-derivative spectrophotometry of complexes with benzoyl-indan-1,3-dione and cetylpyridinium chloride, *Mikrochim. Acta*, 1997, **127**, 71–75, DOI: 10.1007/BF01243167.

16 M. Anbu, T. P. Rao, C. S. P. Iyer and A. D. Damodaran, Simultaneous determination of dysprosium, holmium and erbium in high purity rare earth oxides by second order derivative spectrophotometry, *Chem. Anal.*, 1996, **41**, 781–785.

17 N. X. Wang, Z. K. Si, J. H. Yang and A. Q. Du, Simultaneous determination of neodymium, erbium and holmium in rare earth mixtures with 2-phenyltrifluoroacetone and octylphenol poly(ethyleneglycol) ether by third derivative spectrophotometry, *Talanta*, 1996, **43**, 589–593, DOI: 10.1016/0039-9140(95)01785-2.

18 A. S. Amin, Application of a triacetylcellulose membrane with immobilized of 5-(2`,4`-dimethylphenylazo)-6-hydroxypyrimidine-2,4-dione for mercury determination in real samples, *Sens. Actuators, B*, 2015, **221**, 1342–1347, DOI: 10.1016/j.snb.2015.07.106.

19 N. Hassan and A. S. Amin, Membrane optode for uranium(VI) preconcentration and colorimetric determination in real samples, *RSC Adv.*, 2017, **7**, 46566–46574, DOI: 10.1039/C7RA08942B.

20 A. S. Amin, S. El-Bahy and H. H. El-Feky, Utility of 5-(2′,4′-dimethyl-phenylazo)-6-hydroxy-pyrimidine-2, 4-dione in PVC membrane for a novel green optical chemical sensor to detect zinc ion in environmental samples, *Anal. Biochem.*, 2022, **643**, 114579, DOI: 10.1016/j.ab.2022.114579.

21 A. S. Amin, S. M. El-Bahy and A. M. E. Hassan, Construction of an optical sensor for molybdenum determination based on a new ionophore immobilized on a polymer membrane, *J. King Saud Univ. Sci.*, 2023, **35**, 102592, DOI: 10.1016/j.jksus.2023.102592.

22 M. Aish, R. F. Alshehri, A. S. Amin and E. R. Darwish, Exploring the design and performance of a tellurium optical sensor utilizing a plasticizer-free polymer inclusion membrane, *Food Chem.*, 2024, **439**, 138112, DOI: 10.1016/j.foodchem.2023.138112.

23 S. M. El-Bahy, R. El-Sayed, K. F. Debbabib, A. S. Amin and N. Mohamed, Quantification of tungsten in real samples spectrophoto-metrically using optical sensor, *J. Mol. Liq.*, 2024, **414**, 126104, DOI: 10.1016/j.molliq.2024.126104.

24 N. Hassan, S. El-Bahy, A. O. Babalghith, R. El-Sayed, K. F. Debbabi and A. S. Amin, Development of a high-performance optical sensor for sensitive detection of cobalt ions in pharmaceutical, food, biological, and environmental samples, *Spectrochim. Acta, Part A*, 2025, **327**, 125343, DOI: 10.1016/j.saa.2024.125343.

25 B. Valeur and I. Leray, Design principles of fluorescent molecular sensors for cation recognition, *Coord. Chem. Rev.*, 2000, **205**, 3–40, DOI: 10.1016/S0010-8545(00)00246-0.

26 P. Bühlmann, E. Pretsch and E. Bakker, multispectral imaging of ion transport in neutral carrier-based cation-selective membranes, *Chem. Rev.*, 1998, **98**, 1593–1687, DOI: 10.1021/cr970113+.

27 A. P. De Silva, N. Gunaratne, T. Gunnlaugsson, A. J. M. Huxley, C. P. McCoy, J. T. Rademacher and T. E. Rice, Signaling recognition events with fluorescent sensors and switches, *Chem. Rev.*, 1997, **97**, 1515–1566, DOI: 10.1021/cr960386p.

28 E. Repo, J. K. Warchoł, A. Bhatnagar and M. Sillanpaa, Heavy metals adsorption by novel EDTA-modified chitosan–silica hybrid materials, *J. Colloid Interface Sci.*, 2011, **358**, 261–267, DOI: 10.1016/j.jcis.2011.02.059.

29 S. Yunianti and D. K. Maharani, Pemanfaatan membran kitosan-silika untuk menurunkan kadar ion logam Pb(II) dalam larutan, *U. J. Chem.*, 2012, **1**, 108–115, DOI: 10.26740/ujc.v1n1.p%25p.

30 A. Samadi-Maybodi and V. Rezaei, A new sol–gel optical sensor with nonporous structure for determination of trace zinc, *Sens. Actuators, B*, 2014, **199**, 418–423, DOI: 10.1016/j.snb.2014.03.037.

31 X. Liu, L. Xie and H. Li, Electrochemical biosensor based on reduced graphene oxide and Au nanoparticles entrapped in chitosan/silica sol–gel hybrid membranes for determination of dopamine and uric acid, *J. Electroanal. Chem.*, 2012, **682**, 158–163, DOI: 10.1016/j.jelechem.2012.07.031.

32 A. Yari and H. A. Abdoli, Sol–gel derived highly selective optical sensor for sensitive determination of the mercury(II) ion in solution, *J. Hazard. Mater.*, 2010, **178**, 713–717, DOI: 10.1016/j.jhazmat.2010.01.146.

33 M. R. Ganjali, M. Hosseini, M. Hariri, F. Faridbod and P. Norouzi, Novel erbium(III)-selective fluorimetric bulk optode, *Sens. Actuators, B*, 2009, **142**, 90–96, DOI: 10.1016/j.snb.2009.08.027.

34 Z. Al-Mallah and A. S. Amin, Utilization of a triacetylcellulose membrane to immobilize 5-(2`,4`-dimethyl-phenylazo)-6-hydroxypyrimi-dine-2,4-dione for erbium determination in real sample, *J. Ind. & Eng. Chem.*, 2018, **63**, 281–287, DOI: 10.1016/j.jiec.2018.02.027.

35 N.-X. Wang, L. Wang, W. Jiang, Y.-Z. Ren, Z.-K. Si, X.-X. Qiu, G.-Y. Du and P. Qi, Determination of neodymium, holmium and erbium in mixed rare earths by norfloxacin, *Fresenius. J. Anal. Chem.*, 1998, **361**, 821–824, DOI: 10.1007/s002160051022.

36 D. Ryabchikov and V. Ryabukhin, *Analytical Chemistry for Yttrium and the Lanthanide Elements*, London, Ann, Arbor, 1970.

37 K. Zargoosh and F. F. Babadi, Highly selective and sensitive optical sensor for determination of Pb^{2+} and Hg^{2+} ions based on the covalent immobilization of dithizone on agarose membrane, *Spectrochim. Acta, Part A*, 2015, **137**, 105–110, DOI: 10.1016/j.saa.2014.08.043.

38 Y. M. Scindia, A. K. Pandey, A. V. R. Reddy and S. B. Manohar, Chemically selective membrane optode for Cr(VI) determination in aqueous samples, *Anal. Chim. Acta*, 2004, **515**, 311–321, DOI: 10.1016/j.aca.2004.03.074.

39 H. Harmita, Petunjuk pelaksanaan validasi metode dan cara perhitungannya, *Majalah Ilmu Kefarmasian*, 2004, **1**, 117–135, DOI: 10.7454/psr.v1i3.3375.

40 A. Purwanto, C. Supriyanto and P. Samin, Validasi pengujian Cr, Cu, dan Pb dengan metode spektrometri serapan atom, *Proceeding PPIPDIPTN, Pustek Akselerator Dan Proses Bahan-BATAN*, Yogyakarta, 2007.

41 F. Al-Sagheer and S. Muslim, Thermal and mechanical properties of chitosan/SiO_2 hybrid composites, *J. Nanomater.*, 2010, **2010**, 1–7, DOI: 10.1155/2010/490679.

42 E. J. Lee, D. S. Shin, H. E. Kim, H. W. Kim, Y. H. Koh and J. H. Jang, Membrane of hybrid chitosan–silica xerogel for guided bone regeneration, *Biomaterials*, 2009, **30**, 743–750, DOI: 10.1016/j.biomaterials.2008.10.025.

43 P. Taba, H. Natsir, St. Fauziah and M. Ismail, Adsorpsi ion Cd(II) oleh kitosan-silika mesopori MCM-48, *Marina Chim. Acta*, 2010, **11**, 13–22.

44 R. G. Mudasir, I. Tahir and E. T. Wahyni, Immobilization of dithizone onto chitin isolated from prawn seawater shells and its preliminary study for the adsorption of Cd(II) ion, *J. Phys. Sci.*, 2008, **19**, 63–78.

45 S. Sh. Rashidova, D. Sh. Shakarova, O. N. Ruzimuradov, D. T. Satubaldieva, S. V. Zalyalieva, O. A. Shpigun, V. P. Varlamov and B. D. Kabulov, Bionanocompositional chitosan–silica sorbent for liquid chromatography, *J. Chromatogr., B*, 2004, **800**, 49–53, DOI: 10.1016/j.jchromb.2003.10.015.

46 P. C. A. Jerónimo, A. N. Araújo and M. C. B. S. M. Montenegro, Optical sensors and biosensors based on sol–gel films, *Talanta*, 2007, **72**, 13–27, DOI: 10.1016/j.talanta.2006.09.029.

47 J. H. Mendez, B. M. Cordero and J.-L. Pérez-Pavón, Simultaneous spectrophotometric determination of erbium and praseodymium with 1-(2-pyridylazo)-2-naphthol in the presence of octylphenol poly (ethylene-glycol) ether (TX-100), *Talanta*, 1988, **35**, 293–296, DOI: 10.1016/0039-9140(88)80088-2.

48 A. K. Goswami, Spectrophotometric Determination of Rare Earth Elements: Reagents and Methods, Walter de Gruyter GmbH & Co KG, 2026.

49 M. F. Silva, L. Fernandez, R. A. Olsina and D. Stacchiola, Cloud point extraction, preconcentration and spectrophotometric determination of erbium(III)-2-(3,5-dichloro-2-pyridylazo)-5-dimethylaminophenol, *Anal. Chim. Acta*, 1997, **342**, 229–238, DOI: 10.1016/S0003-2670(96)00603-4.

50 N.-X. Wang, J.-H. Yang, H. Siu and P. Qi, Third-derivative spectro-photometric determination of neodymium and erbium in mixed rare earths with 2-(diphenylacetyl) indan-1,3-dione and dodecyl benzenesulfonic acid sodium salt, *Analyst*, 1995, **120**, 2413–2416, DOI: 10.1039/AN9952002413.

51 J. D'Angelo, J. Fernandez, L. Martinez and E. J. Marchevsky, Sensitive spectrophotometric determination of erbium(III) in geological materials and glasses with 2-(5-bromo-2-pyridylazo)-5-diethylaminophenol, *J. Anal. Chem.*, 1999, **54**, 665–669.

52 J. N. Miller and J. C. Miller, *Statistics and Chemometrics for Analytical Chemistry*, Prentice-Hall, London, 5th edn, 2005.

53 M. Gasgnier, Rare-earth elements in permanent magnets and superconducting compounds and alloys (except new high Tc ceramics) as thin films, thin crystals and thinned bulk materials, *J. Mater. Sci.*, 1991, **26**, 1989–1999, DOI: 10.1007/BF00549157.

54 F. Herbst and J. J. Croat, Neodymium-iron-boron permanent magnets, *J. Magn. Magn. Mater.*, 1991, **100**, 57, DOI: 10.1016/0304-8853(91)90812-O.